Research Article | Vol. 25, No. 15 | 24 Jul 2017 | OPTICS EXPRESS 18332
Optics EXPRESS

Optimization of morphological parameters for mitigation pits on rear KDP surface: experiments and numerical modeling

HAO YANG,[1,2,3] JIAN CHENG,[1,3] MINGJUN CHEN,[1,*] JIAN WANG,[2] ZHICHAO LIU,[2] CHENHUI AN,[2] YI ZHENG,[2] KEHUI HU,[1] AND QI LIU[1]

[1]State Key Laboratory of Robotics and System, Harbin Institute of Technology, Harbin 150001, China
[2]Research Center of Laser Fusion, China Academy of Engineering Physics, Mianyang 621900, China
[3]These authors contributed equally to this work
[*]chenmj@hit.edu.cn

Abstract: In high power laser systems, precision micro-machining is an effective method to mitigate the laser-induced surface damage growth on potassium dihydrogen phosphate (KDP) crystal. Repaired surfaces with smooth spherical and Gaussian contours can alleviate the light field modulation caused by damage site. To obtain the optimal repairing structure parameters, finite element method (FEM) models for simulating the light intensification caused by the mitigation pits on rear KDP surface were established. The light intensity modulation of these repairing profiles was compared by changing the structure parameters. The results indicate the modulation is mainly caused by the mutual interference between the reflected and incident lights on the rear surface. Owing to the total reflection, the light intensity enhancement factors (LIEFs) of the spherical and Gaussian mitigation pits sharply increase when the width-depth ratios are near 5.28 and 3.88, respectively. To achieve the optimal mitigation effect, the width-depth ratios greater than 5.3 and 4.3 should be applied to the spherical and Gaussian repaired contours. Particularly, for the cases of width-depth ratios greater than 5.3, the spherical repaired contour is preferred to achieve lower light intensification. The laser damage test shows that when the width-depth ratios are larger than 5.3, the spherical repaired contour presents higher laser damage resistance than that of Gaussian repaired contour, which agrees well with the simulation results.

OCIS codes: (140.3330) Laser damage; (220.4610) Optical fabrication; (160.4330) Nonlinear optical materials.

References and links

1. K. R. Manes, M. L. Spaeth, J. J. Adams, and M. W. Bowers, "Damage mechanisms avoided or managed for NIF large optics," Fus. Sci. Technol. **69**(1), 146–249 (2016).
2. R. Hawley-Fedder, P. Geraghty, S. Locke, M. McBurney, M. Runkel, T. Suratwala, S. Thompson, P. Wegner, and P. Whitman, "NIF Pockels cell and frequency conversion crystals," Proc. SPIE **5341**, 121–126 (2004).
3. J. J. De Yoreo, A. K. Burnham, and P. K. Whitman, "Developing KH_2PO_4 and KD_2PO_4 crystals for the world's most power laser," Int. Mater. Rev. **47**(3), 113–152 (2002).
4. S. Reyné, G. Duchateau, J. Y. Natoli, and L. Lamaignère, "Laser-induced damage of KDP crystals by 1ω nanosecond pulses: influence of crystal orientation," Opt. Express **17**(24), 21652–21665 (2009).
5. P. A. Baisden, L. J. Atherton, R. A. Hawley, and T. A. Land, "Large optics for the national ignition facility," Fus. Sci. Technol. **69**(1), 614–620 (2016).
6. J. H. Campbell, R. A. Hawley-Fedder, C. J. Stolz, J. A. Menapace, M. R. Borden, P. K. Whitman, J. Yu, M. J. Runkel, M. O. Riley, M. D. Feit, and R. P. Hackel, "NIF optical materials and fabrication technologies: an overview," Proc. SPIE **5341**(10), 84–101 (2004).
7. M. A. Norton, J. J. Adams, C. W. Carr, E. E. Donohue, M. D. Feit, R. P. Hackel, W. G. Hollingsworth, J. A. Jarboe, M. J. Matthews, A. M. Rubenchik, and M. L. Spaeth, "Growth of laser damage in fused silica: diameter to depth ratio," Proc. SPIE **6720**, 67200H (2007).
8. S. G. Demos, M. R. Kozlowski, M. Staggs, L. L. Chase, A. Bumham, and H. B. Radousky, "Mechanisms to explain damage growth in optical materials," Proc. SPIE **4347**, 277–284 (2001).
9. S. G. Demos, R. A. Negress, R. N. Raman, A. M. Rubenchik, and M. D. Feit, "Material response during nanosecond laser induced breakdown inside of the exit surface of fused silica," Laser Photonics Rev. **7**(3), 444–452 (2013).

#296343 https://doi.org/10.1364/OE.25.018332
Journal © 2017 Received 19 May 2017; revised 24 Jun 2017; accepted 7 Jul 2017; published 20 Jul 2017

Optics EXPRESS

10. S. R. Qiu, J. E. Wolfe, A. M. Monterrosa, M. D. Feit, T. V. Pistor, and C. J. Stolz, "Searching for optimal mitigation geometries for laser-resistant multilayer high-reflector coatings," Appl. Opt. **50**(9), C373–C381 (2011).
11. M. L. Spaeth, P. J. Wegner, T. I. Suratwala, and M. C. Nostrand, "Optics recycle loop strategy for NIF operations above UV laser–induced damage threshold," Fus. Sci. Technol. **69**(1), 265–294 (2016).
12. L. W. Hrubesh, R. M. Brusasco, W. Grundler, M. A. Norton, E. E. Donohue, W. A. Molander, S. L. Thompson, S. R. Strodtbeck, P. K. Whitman, M. D. Shirk, P. J. Wegner, M. C. Nostrand, and A. K. Burnham, "Methods for mitigating growth of laser-initiated surface damage on DKDP optics at 351 nm," Proc. SPIE **4932**, 180–191 (2003).
13. R. A. Negres, S. O. Kucheyev, P. DeMange, C. Bostedt, T. Van Buuren, A. J. Nelson, and S. G. Demos, "Decomposition of KH_2PO_4 crystals during laser-induced breakdown," Appl. Phys. Lett. **86**(17), 171107 (2005).
14. C. J. Stolz, "The national ignition facility: the path to a carbon-free energy future," Philos Trans A Math Phys Eng Sci **370**(1973), 4115–4129 (2012).
15. I. L. Bass, G. M. Guss, M. J. Nostrand, and P. J. Wegner, "An improved method of mitigating laser–induced surface damage growth in fused silica using a rastered pulsed CO_2 laser," Proc. SPIE **7842**(1), 784220 (2010).
16. P. Geraghty, W. Carr, V. Draggoo, R. Hackel, C. Mailhiot, and M. Norton, "Surface damage growth mitigation on KDP/DKDP optics using singl–ecrystal diamond micro–machining ball end mill contouring," Proc. SPIE **6403**, 64030Q (2006).
17. J. Cheng, M. Chen, W. Liao, H. Wang, Y. Xiao, and M. Li, "Fabrication of spherical mitigation pit on KH_2PO_4 crystal by micro-milling and modeling of its induced light intensification," Opt. Express **21**(14), 16799–16813 (2013).
18. M. J. Chen, J. Cheng, X. D. Yuan, W. Liao, H. J. Wang, J. H. Wang, Y. Xiao, and M. Q. Li, "Role of tool marks inside spherical mitigation pit fabricated by micro-milling on repairing quality of damaged KH_2PO_4 crystal," Sci. Rep. **5**(1), 14422 (2015).
19. N. L. Boling, M. D. Crisp, and G. Dubé, "Laser induced surface damage," Appl. Opt. **12**(4), 650–660 (1973).
20. Y. Xiao, M.-J. Chen, J. Cheng, W. Liao, H.-J. Wang, and M.-Q. Li, "Effect of structural parameters of Gaussian repaired pit on light intensity distribution inside KH2PO4 crystal," Chin. Phys. B **23**(8), 540–547 (2014).
21. J. M. Jin and J. G. Wang, *Finite Element Method in Electromagnetic Field* (Xi'an Electronic and Science University, 1998).
22. N. L. Boling, G. Dubé, and M. D. Crisp, "Morphological asymmetry in laser damage of transparent dielectric surfaces," Appl. Phys. Lett. **21**(10), 487–489 (1972).
23. L. Li, X. Xiang, X.-T. Zu, X.-D. Yuan, S.-B. He, X.-D. Jiang, and W.-G. Zheng, "Incident laser modulation of a repaired damage site with a rim in fused silica rear subsurface," Chin. Phys. B **21**(4), 351–356 (2012).
24. L. Hrubesh, J. J. Adams, M. D. Feit, W. D. Sell, J. A. Stanley, E. Miller, S. L. Thompson, P. K. Whitman, and R. P. Hackel, "Surface damage growth mitigation on KDP/DKDP optics using single–crystal diamond micromachining," Proc. SPIE **5273**, 273–280 (2004).
25. F. Y. Génin, A. Salleo, T. V. Pistor, and L. L. Chase, "Role of light intensification by cracks in optical breakdown on surfaces," J. Opt. Soc. Am. A **18**(10), 2607–2616 (2001).
26. J. Wong, J. L. Ferriera, E. F. Lindsey, D. L. Haupt, I. D. Hutcheon, and J. H. Kinney, "Morphology and microstructure in fused silica induced by high fluence ultraviolet 3ω (355 nm) laser pulses," J. Non-Cryst. Solids **352**(3), 255–272 (2006).
27. C. W. Carr, M. D. Feit, M. A. Johnson, and A. M. Rubenchik, "Complex morphology of laser-induced bulk damage in $K_2H_{(2-x)}D_xPO_4$ crystals," Appl. Phys. Lett. **89**(13), 131901 (2006).

1. Introduction

Due to the unique optical performance, KDP crystals, serving as terminal frequency converters and optical switch-Pockels cells, have been widely applied in high power laser systems, such as National Ignition Facility (NIF) in USA, Laser MegaJoule (LMJ) in France and SG-III Laser Facility in China [1–5]. During the processes of ultra-precision machining and high-fluence laser irradiation, tiny defects (e.g., cracks, fracture and ablation) are generated inevitably due to the weak mechanical properties (soft and brittle) of KDP material, vibration of machine tool, and subsequent flaw-induced "explosion" of laser damage [2,6,7]. These defects have been regarded as the origins of nonlinear heat absorption, enhanced scattering and light intensification, which should be responsible for the "re-ignition" and growth of damage sites under subsequent laser irradiations. Hence, these defects would sharply reduce the laser-induced damage threshold (LIDT), affect the optical transmission and finally shorten the life time of KDP crystal, especially when they are located on the rear surface [1,8,9]. Due to the time-consuming growth period, great processing difficulty and high manufacturing cost of large aperture KDP crystal, it is a good way to repair the optical component by replacing the original defects with smooth contours [2,3,10]. The "optical

Optics EXPRESS

recycle loop strategy" was firstly proposed by Lawrence Livermore National Laboratory through a routine work of assessing and repairing the surface damage or exchanging the optical components regularly [11]. Comparing the current potential methods for the mitigation of KDP crystal surface defects like CW-CO_2 laser processing, aqueous wet-etching, short-pulse laser ablation and micro-machining, it has been concluded that micro-machining is the most promising approach to mitigate the laser damage growth for KDP crystal due to its complete controllability for fabricating different mitigation contours [12].

Two main points to repair the surface defects are reducing the defect-induced light intensification inside the crystal to prevent damage growth, and guaranteeing low interference and convergence possibility of downstream light [13,14]. Based on finite difference time domain (FDTD) method, Qiu et al. [10] investigated the light intensity distribution inside the optics induced by conical mitigation contours on multilayer high reflector coatings. The results verified the dependence of light intensification on incident angle, polarization direction of laser, and cone angle of mitigation contour. Bass et al. [15] proposed a new technique, using a rastered, pulsed CO_2 Laser, to prevent the formation of a raised rim around the final mitigation site and its consequent down-stream intensification. Geraghty et al. [16] proposed a micro-milling method with ball-end cutter for damage mitigation on KDP crystal and found that the growth behavior of surface damage would be substantially mitigated when single crystal diamond tool is applied to repair the initial damage site. Cheng et al. [17] calculated the Maxwell curl equation using FDTD method, and verified the feasibility of mitigation pits with spherical contour for mitigating the light intensification near the surface damage site. Moreover, the experiment results indicated that the spherical mitigation pits repaired with micro-machining method was able to achieve LIDT two-fold higher than that of initial damage site.

Currently, spherical and Gaussian mitigation pits have been considered to be effective to mitigate the growth of the damage sites on KDP crystal surface [16,17]. Although tool marks produced by micro-milling with several nanometers height on the surface of mitigation pits would generate diffraction and field enhancement effects [18], these negative effects could be controlled by optimizing the machining parameters during the repairing processes. However, in engineering practice, how to choose the repaired contour and structure parameters of the mitigation pit has not been reported. In this work, based on electromagnetic theory, the models for simulating the light intensification caused by spherical and Gaussian mitigation pit on rear surface of KDP crystal were established using finite element method (FEM). We studied the effect of structure parameters (width and depth) of mitigation pits on the light intensification inside the KDP crystal, analyzed the primary cause for the light field modulation by mitigation pit with different width-depth ratios, and proposed the optimum technological parameters for machining process according to the simulation results. Besides, four series of mitigation pits with various shapes and dimensions were fabricated by micro-milling with a ball end milling cutter. The laser damage test was performed as well on the machined mitigation sites, and the tested LIDTs were well consistent with the simulation results. In a word, this work is focused on the comparison of repairing effectiveness between the fabricated spherical and Gaussian mitigation pits. A criterion for optimizing the repairing structure parameters of these two kinds of mitigation pits was proposed by considering the light interference in the vicinity of these repaired mitigation contours.

2. Model and theory

Under high power laser irradiation, the defects (e.g., cracks, fracture and ablation) on the KDP surface would produce light field modulation inside the crystal, especially in the case that the defects are located on the rear surface [12,19]. Our previous work [17,20] indicated that the repaired smooth surfaces with spherical and Gaussian contours would largely mitigate the light field modulation inside KDP crystal. In this work, the finite element method (FEM) was utilized to model a series of spherical and Gaussian pits with different widths and depths,

Optics EXPRESS

which are shown in Fig. 1. Figure 1(a) is the 3D model, and Figs. 1(b) and 1(c) illustrate the vertical cross-sections of the spherical and Gaussian pits, respectively. The spherical curve and Gaussian curve can be denoted as Eqs. (1) and (2).

$$x^2 + (z - (R - d))^2 = R^2 \tag{1}$$

$$z = -d \cdot \exp(-16x^2 / w^2) \tag{2}$$

where d and w are the depth and width of the mitigation pits. The radius of spherical curve R can be calculated by

$$R = 0.5d + 0.125w^2 / d \tag{3}$$

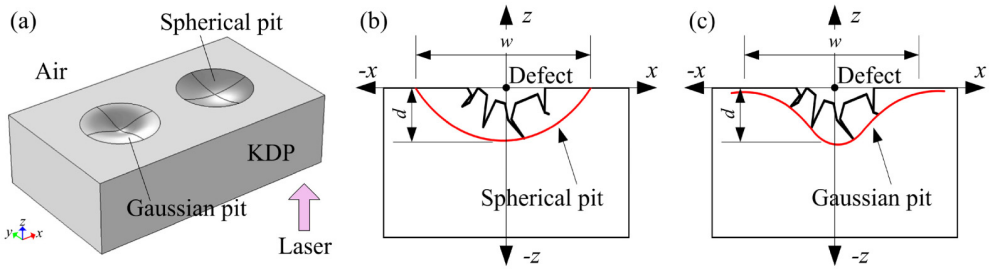

Fig. 1. Schematic diagrams of repaired mitigation pits on KDP surface. (a) 3D model for mitigation pits. (b) Cross-section of spherical mitigation pit. (c) Cross-section of Gaussian mitigation pit.

Since light is a special kind of electromagnetic wave, the frequency domain analysis of FEM was adopted in the model. Incident wave was simplified as harmonic plane electromagnetic wave with TE mode due to its more serious modulation effect than that of TM mode [17]. The electric field intensity was normalized to 1V/m. Therefore, the Helmholtz Eq. (4) can be chosen as the governing equation [21].

$$\nabla \times (\nabla \times E) - k^2 \varepsilon_r E = 0 \tag{4}$$

Here, E is the electric field intensity, k is the wave number, ε_r is the relative dielectric constant and ∇ denotes the differential operator.

The FEM models need enough mesh generation for precise simulation results. In order to reduce the calculation memory and enhance the solving efficiency, the models only include 2D cross-sections, as shown in Fig. 2. Figures 2(a) and 2(b) are simulation models for spherical and Gaussian mitigation pits, respectively. In each model, the overall width is 30μm, and the heights of top-layer air and sub-layer KDP are 4μm and 20μm, respectively. The 2ω (λ = 532nm) plan wave irradiates along the + z axis with the direction normal to the front surface AB of the KDP crystal. The surfaces of AB and CD apply the scattering boundary conditions (SBC), which is perfectly transparent for scattered (incoming and outgoing) waves at normal incidence to the boundary. In order to realize the plane wave, the surfaces of AD and BC apply the periodic boundary conditions (PBC). For KDP crystal, the birefringence is ignored in this model. Under the temperature of 20°C and light wavelength of 532nm, the relative dielectric constant ε_r is 1.512 (n^2_{KDP}), and two other electromagnetic parameters of relative magnetic permeability μ_r and electric conductivity σ are 1.0 and 0, respectively.

Optics EXPRESS

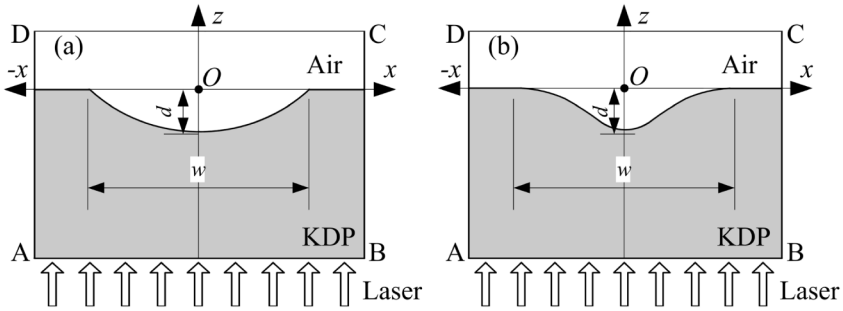

Fig. 2. 2D models of mitigation pit. (a) Spherical mitigation pit. (b) Gaussian mitigation pit.

The distribution of electric field intensity is relatively uniform with the plan wave normalized to 1V/m irradiating from air to ideal KDP surface (no repaired contours) in the normal direction [Fig. 3]. Some ripples with low amplitude appear in the KDP region. The average electric field intensity there is approximately 0.8026 V/m with the error less than 0.1%, when compared to the analytically calculated one (0.8032V/m) according to the Fresnel reflection theory [22]. Thus the validity and feasibility of the FEM model is well proved.

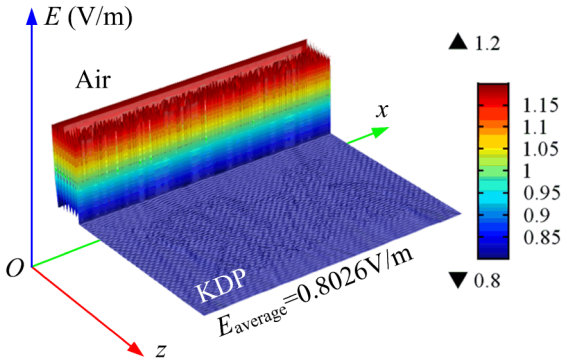

Fig. 3. Distribution of electric field intensity with the plan wave normalized to 1V/m irradiating from air to ideal KDP surface in the normal direction.

Light intensification is the main cause, leading to the laser damage growth of fused silica and nonlinear crystals [23]. Once it exceeds a critical value, multiphoton ionization and impact ionization would occur. The heat absorption of free electron would also deteriorate the environment of laser transmission [1]. Therefore, light intensity enhancement factor (LIEF) is introduced to indicate the laser damage resistance of KDP crystal with repaired contours [17].

$$LIEF = I_{max} / I_0 \tag{5}$$

where I_{max} is the largest light intensity inside the KDP crystal with repaired contours, and I_0 is the light intensity inside the KDP crystal with ideal surface. The larger LIEF is, the more easily laser damage would occur or grow. For the incident plane wave, the light intensity is proportional to the square of electrical field ($|E|^2$), which means that the calculated results of electric field intensity by the FEM models can be directly applied in Eq. (5).

For KDP crystal irradiated by 532nm plane wave (n = 1.51), total reflection would occur at specific locations on mitigation pits, where the incident angles (α_i) are larger than 41.5°. For α_i larger than 45° and smaller than 69.3°, the incident light is totally reflected at both mitigation pit and output surface (double total reflection, DTR for short). The reflected light could interact with the incident light, and then increase the possibility of light intensification.

Optics EXPRESS

For α_i larger than 69.3°, some light transmits into the air from the rear surface, which could reduce the degree of light intensification inside the KDP crystal.

The incident light at different locations of mitigation pits gets different incident angles (α_i), which share a tangent relationship with the slopes (k_i) of the mitigation contour. Figure 4 is the schematic of total reflection. When the light rays are sent between the positions of a and b, no total reflection would occur. The c and d show the cases of double total reflection in the graphs, which are corresponding to the slope k_i of 1 and 2.65, respectively. The ray of e is taken as an example of the transmission light from rear KDP surface. The largest slope $k_{S,max}$ for spherical pits is located at the highest point of the pit given by Eq. (6). And Eq. (7) refers to the largest slope $k_{G,max}$ of Gaussian pits.

$$k_{S,\max} = \frac{4wd}{w^2 - 4d^2} = \frac{4\zeta}{\zeta^2 - 4} \tag{6}$$

$$k_{G,\max} = \frac{1}{\zeta} \cdot 4\sqrt{2}e^{-0.5} \tag{7}$$

where w and d are the width and depth of mitigation pits. The width-depth ratio $\zeta = w/d$.

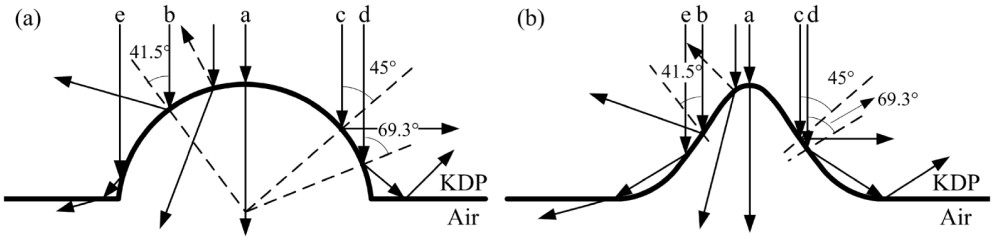

Fig. 4. Schematic of total reflection at the repaired surfaces. (a) Spherical mitigation pit. (b) Gaussian mitigation pit.

The morphology of mitigation pit determines the range of incident angle, which could be applied to estimate whether the total reflection occurs or not. As for spherical mitigation pits, for $\zeta > 5.28$, no total reflection occurs. But there would be double total reflections among the range of 2.89 and 4.83. As for Gaussian mitigation pits, no total reflection and double total reflection occur at the condition of $\zeta > 3.88$ and $\zeta \in (1.30, 3.43)$, respectively.

3. Fabrication of mitigation pits and laser damage experiment

A self-developed multi-axis micro-milling machine is employed to repair the surface flaws on KDP crystal surfaces. Figure 5 is the schematic of machining process for repairing the surface flaws with micro-machining method [16,24]. The fabrication method of multi-path milling is applied in this repairing work, which is more flexible to fabricate complex contours than our previous work [17]. The double-edged ball-end micro cutter (SSBL200), made from CBN (cubic boron nitride) material, is adopted and the ball diameter D is 500μm. The tilted angle between crystal surface and the rotary cutter axis should be larger than 30° to ensure ductile-mode cutting of brittle KDP materials [20]. During the machining process, the spindle speed is 50,000 RPM, and the tilted angle is maintained at 45°. The cutter is set at the bottom of the crystal so that the chip of cut KDP material can be discharged easily.

Optics EXPRESS

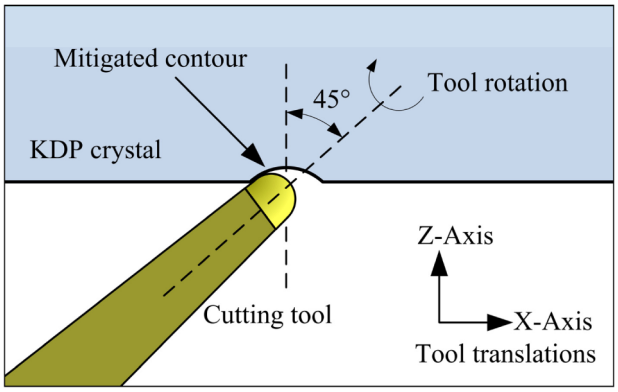

Fig. 5. Schematic of the machining process for repairing the surface flaws on KDP crystal with micro-machining method.

A total of four series of mitigation pits were fabricated, including spherical mitigation pits with 1000μm width and 50μm depth, spherical mitigation pits with 500μm width and 50μm depth, Gaussian mitigation pits with 1000μm width and 50μm depth and Gaussian mitigation pits with 500μm width and 50μm depth. Figure 6 exhibits the stereoscopic microscopic images of the four series of mitigation pits. It is shown that the overall internal surfaces of the mitigation pits are smooth and the processing texture distributes uniformly. The insets in Fig. 6 are the cross-sectional profiles of the fabricated mitigation pits tested using surface profiler. One can see that the fabricated spherical and Gaussian contours are well consistent with the Spherical and Gaussian curves derived from Eqs. (1) and (2). The surface roughness Ra of the fabricated mitigation contours are all below 30nm, which satisfies the requirement of the surface quality for the optical element mitigation project. It is worth noting that the initially damaged surface is extremely rough, which consists of various defects.

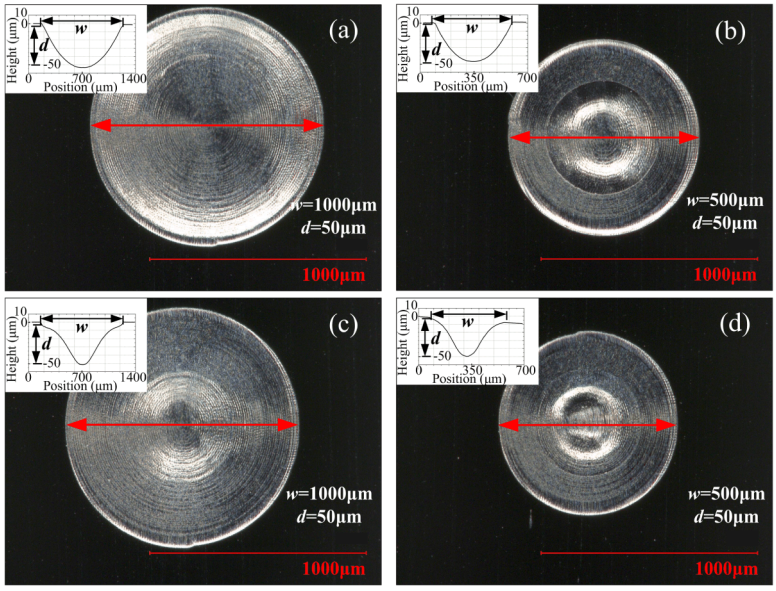

Fig. 6. Stereoscopic images of fabricated mitigation pits on KDP crystals and the insets are the cross-sectional profiles of the fabricated mitigation pits tested using surface profiler. (a) The spherical mitigation pit with 1000μm width and 50μm depth. (b) The spherical mitigation pit with 500μm width and 50μm depth. (c) The Gaussian mitigation pit with 1000μm width and 50μm depth. (d) The Gaussian mitigation pit with 500μm width and 50μm depth.

Optics EXPRESS

Figure 7 shows the diagram of light path for testing the LIDTs of KDP crystal. The high energy laser in the experimental system is provided by a single longitudinal mode Nd: YAG SAGA laser, which can output steady pulse laser with wavelengths of 1064nm, 532nm and 355nm. In the testing experiment, double frequency laser of 532nm is utilized, with 1Hz repetition rate and 10ns pulse duration. The output laser energy has a spatial distribution of Gaussian profile on the rear surface of the crystal with the effective spot area of 0.711mm^2. The surface with fabricated mitigation pits is set as the output surface of the laser beams. In order to achieve a flat laser intensity profile for guaranteeing the equal laser irradiation intensity, rapid raster scan of the focused beam was performed on the whole repaired mitigation pits. After every cycle of scanning, the laser pulse would be changed with a higher fluence. Based on the ramped-fluence multiple-shot test (R-on-1) protocol, the damage fluence is defined as the lowest fluence at which any damage is observed on the rear surface of the sample. The LIDT is the average damage fluence of the tested spots.

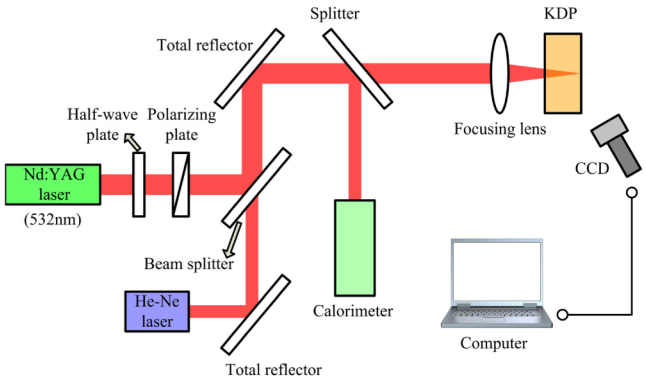

Fig. 7. Diagram of light path for testing the LIDTs of KDP crystal.

4. Results and discussion

The following sections are four-fold. The first two parts are focused on the analysis of the light modulation results of spherical and Gaussian mitigation pits. In the third part, we compared the LIEFs between spherical and Gaussian mitigation pits, and discussed the repair effect under different morphology with constant width-depth ratio. Those analyses play significant role in the future repairing work to choose the optimum structure parameters of mitigation pits. In the last part, the LIDT test is implemented to verify the efficiency of simulation results.

4.1 Width and depth effect of spherical mitigation pits on light intensity enhancement

Most incident light would transmit through the rear surface of KDP on the ideal conditions with no surface features. However, for KDP surface with mitigation pits, some reflected light would change their original orientation, which leads to the interference inside the crystal, especially when the total reflection occurs. The simulated interference patterns are shown in Fig. 8, where the distribution of electric field intensity E is conveyed. It is found that electric field intensity E inside the crystal distributes symmetrically with respect to the axis of $z = 0$. In Fig. 8(a), the width-depth ratio ζ of the spherical mitigation pit is 50 (larger than 5.28, the critical width-depth ratio for the occurrence of total reflection), which produces a relatively uniform electric field distribution and lower intensity modulation with the largest E of 1.31V/m and lowest LIEF of 1.19 inside the crystal. The diffraction ripples with low amplitude appear in some regions with low E. In Fig. 8(b), for the width-depth ratio ζ of 3.33, located between 2.89 and 4.83, the DTR occurs on the rear surface. Electric field intensity gets modulated seriously with the maximum E of 3.86 V/m and LIEF of 10.32. With the serious light intensification, laser damage may occur catastrophically under high fluence laser

Optics EXPRESS

irradiation [25]. These mitigation pits with violent light intensity modulation are not expected to be applied in the actual repairing process. On the other hand, the hot spots depicted in red color distribute dispersedly like flake clouds. The spots with maximum electric field intensity are mainly distributed below the top point of spherical repaired contour and at the intersection zone of the repaired contour and rear surface. Without half-wave loss on KDP rear surface during the reflection process (KDP crystal is a sort of light medium with higher optical density toward the outside air), the phase of reflected light is the same as that of the incident light at the reflection points, which would generate standing waves and amplitude doubling. It is probably the reason why the maximum spots appear on the rear surface and the laser damage there grows more rapidly.

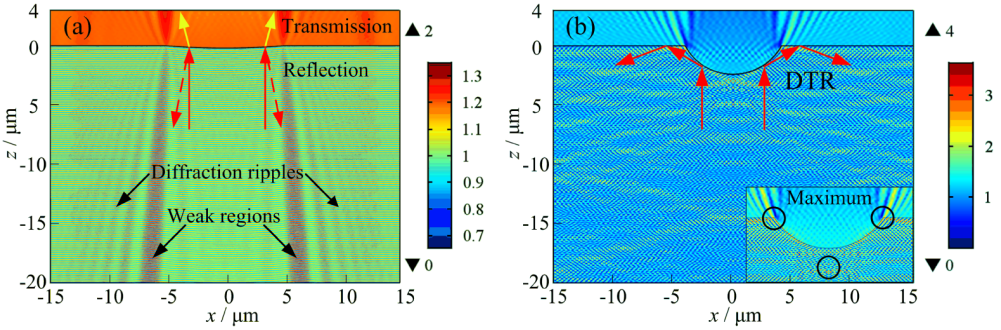

Fig. 8. Modulation of electric field intensity caused by rear surface spherical mitigation pit. (a) $w = 10\mu m$, $d = 0.2\mu m$. (b) $w = 8\mu m$, $d = 2.4\mu m$.

Figure 9(a) shows the curves of LIEFs as a function of repairing depth with three different widths of spherical mitigation contours. It can be seen that the three curves with the widths of 6μm, 8μm and 10μm have a similar trend. With the increase of the depth, the LIEFs inside the crystal rise generally. When the width-depth ratios of the spherical mitigation pits are greater than 5.28 (i.e., $w = 6\mu m$, $d < 1.2\mu m$; $w = 8\mu m$, $d < 1.6\mu m$; $w = 10\mu m$, $d < 1.8\mu m$), these three curves are almost overlapped with relative smaller slopes. When the width-depth ratio ζ exceeds the critical value of 5.28, the slopes of the three curves change abruptly with the rapidly increasing LIEFs. According to the total reflection analysis of the spherical mitigation pit as depicted in Fig. 4(a), one can see that the slope change of the three curves here is caused by the total reflection at the rear surface, which is further confirmed by our previous work (see Ref [17].). The two curves with widths of 6μm and 8μm reach the summits at the depths of 2.0μm and 2.4μm, respectively. The LIEFs begin to decrease with the increase of the depth afterward. Based on the aforementioned analysis of the total reflection, when the width-depth ratio ζ is less than 2.89, a part of the light would transmit from the rear surface of the crystal. Thus, the curves start to show a downward trend when the ζ is smaller than 2.89. With the limitation of the inclination angle for cutting tools during the repairing process, machining interference would occur when repairing depth is rather large. Hence, the excessive depth dimensions are no longer discussed in this work. Figure 9(b) shows the relationship between LIEFs and the width-depth ratio ζ of spherical mitigation pits without the effect of total reflection. These three curves with different widths are almost parallel, descending as the width-depth ratios increase and arranged from the top to the bottom in order of width. In other words, the LIEF would be affected by the size of repaired contour that the larger the size is, the greater the LIEF would be. It is the reason why the maximum value of the 8μm-width curve is larger than that of the 6μm-width curve in the Fig. 9(a). Additionally, when the width-depth ratio ζ is close to the critical value of 5.28, these three curves are approximately vertical. It can be concluded that the spherical contours with width-depth ratios larger than 5.3 are suitable for the mitigation of laser damage growth, which would reduce the light field modulation inside the crystal and enhance the laser damage

Optics EXPRESS

resistance. With the same width-depth ratio, the LIEFs would increase with the increasing size of the repaired pits. So in the repairing process, both the effects of width-depth ratio and the size of repaired contours on the light field modulation should be considered to determine the optimum structure parameters of the mitigation pits.

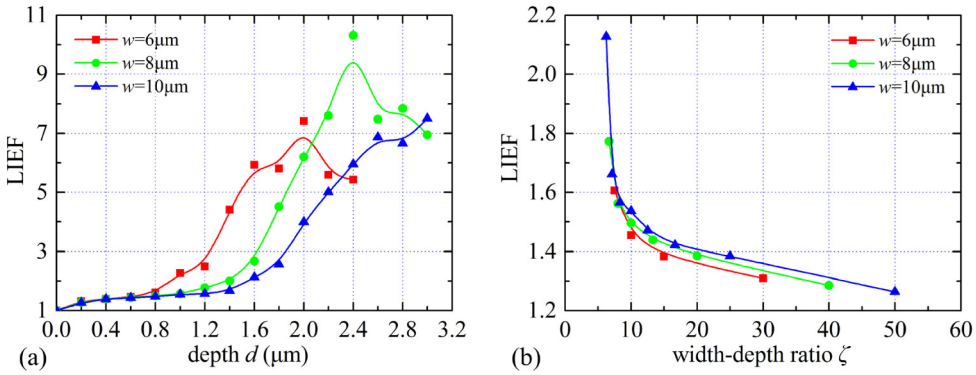

Fig. 9. Evolution of LIEFs versus structural parameters of spherical mitigation contours. The curves of LIEFs caused by spherical mitigation pit with three widths as a function of depth (a) and width-depth ratio (b).

4.2 Width and depth effect of Gaussian mitigation pits on light intensity enhancement

Figure 10 shows the modulation of electric field intensity caused by Gaussian mitigation pit on the rear surface. The width-depth ratio of the repaired pit in Fig. 10(a) is 50, which is greater than 3.88 (the critical width-depth ratio for the occurrence of total reflection). Hence, the total reflection does not occur inside the KDP crystal. The maximum value of the electric field intensity is 1.35V/m and the corresponding LIEF is 1.27. The diffraction patterns inside the crystal caused by spherical and Gaussian repaired pits with large width-depth ratio are similar, except for the area of diffraction ripples. For the Gaussian pits in Fig. 10(a), there is a narrower region of ripples than that for spherical pits in Fig. 8(a). Figure 10(b) exhibits the simulation results of Gaussian mitigation pit with the width-depth ratio of 2.67, located between 1.30 and 3.43, which would lead to the DTR inside the crystal. The maximum value of electric field intensity inside the crystal generated by Gaussian contour is 4.36V/m and the LIEF reaches 13.18. These spots mainly distributes at the positions of the waist (maximum slope) of the contour as well as their neighboring regions at both sides of the top point. Besides, instead of appearing at the junction of the repaired contour and unrepaired surface like that of the spherical mitigation pits, the distribution of other maximum spots for Gaussian pits are present at a parallel area in a certain depth from the rear surface. These hot spots are the potential source to induce the laser damage.

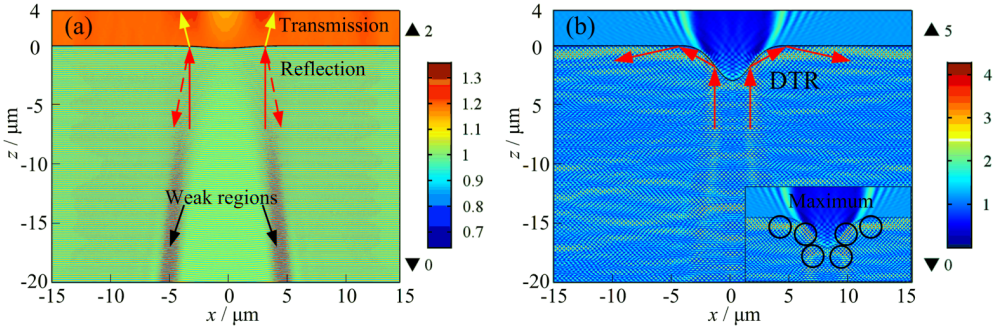

Fig. 10. Modulation of electric field intensity caused by rear surface Gaussian mitigation pit. (a) w = 10μm, d = 0.2μm. (b) w = 8μm, d = 3μm.

Optics EXPRESS

Figure 11(a) shows the curves of LIEFs as a function of repair depth with three constant widths of Gaussian mitigation contours. It can be seen that the LIEFs of the three curves exhibit an overall increasing trend with increase of the repairing depth. When the width-depth ratios of the Gaussian mitigation pits are greater than 3.88 (i.e., w = 6μm, d <1.4μm; w = 8μm, d <2.0μm; w = 10μm, d = 2.4μm), the three curves increase slowly and almost share the same growth rate. With the width-depth ratio less than 3.88, the LIEFs rise sharply, and the slopes of these three curves are still approximately equal after the turning point. According to the results of the total reflection analysis of Gaussian mitigation pit as described in Section 2, there is no doubt that the total reflection on the rear surface is the main reason for the sudden change of the curve slope. It can be deduced that when the width-depth ratio is less than 1.30, the curve would begin to show a decreasing trend. However, such a deep pit with a small width-depth ratio is extremely difficult to machine in the actual repairing process. Figure 11(b) is the relationship between LIEF and the width-depth ratio ζ of Gaussian contour without the effect of total reflection. It shows that the Gaussian morphology has the same rule as the spherical morphology. The three curves are almost parallel and the LIEFs inside the crystal would increase as the repair size increased. The three curves are almost perpendicular with the width-depth ratio ζ near 3.88. Therefore, parameters of the width-depth ratio not less than 3.9 and the size as small as possible are recommended for the application of defect repairing with Gaussian contour.

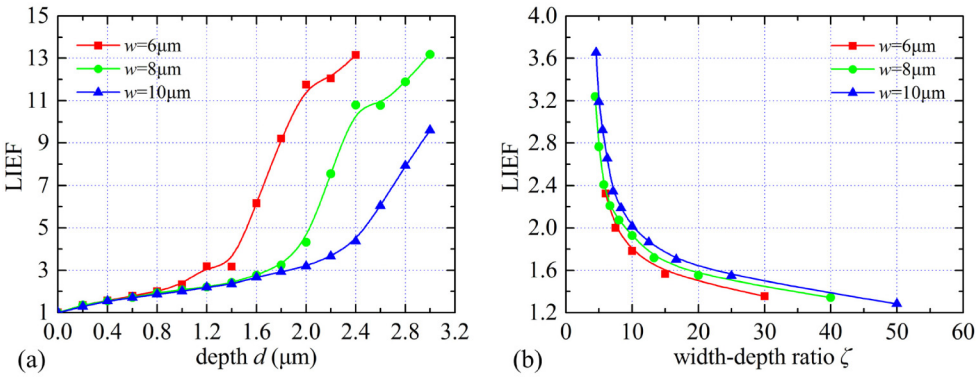

Fig. 11. Evolution of LIEFs versus structural parameters of Gaussian mitigation contours. The curves of LIEFs caused by Gaussian mitigation pit with three widths as a function of depth (a) and width-depth ratio (b).

4.3 Morphology effect of mitigation pits on light intensity enhancement

For the rear surface with different morphology of spherical and Gaussian repair pits, the induced light intensity modulation inside the crystal varies from each other. Figures 12 are the variations of LIEFs caused by spherical and Gaussian mitigation pits with respect to the repairing depth for the width of 6μm, 8μm and 10μm. It can be found that there is an intersection point for every two curves, with the corresponding width-depth ratio to be approximately 5. When the width-depth ratios are larger than 5, the LIEFs of the spherical mitigation pits are smaller than those of the Gaussian pits. When the width-depth ratios are less than 5, the LIEFs of the spherical mitigation pits would increase rapidly, and the LIEFs of the Gaussian mitigation pits are smaller. Introduce a critical value of LIEF = 4 for the recommended repaired contour. Observing the curves of the Gaussian mitigation pits in the three graphs, when the width-depth ratios are larger than 4.3, the LIEFs are all lower than 4 for all the Gaussian mitigation pits with the width of 6μm, 8μm and 10μm. So in order to ensure the reliability of Gaussian mitigation pits, it is recommended to repair the defects into a Gaussian contour with width-depth ratio more than 4.3. According to the results of Section 3.1, the width-depth ratios larger than 5.3 are recommended for the spherical mitigation pit. In

Optics EXPRESS

a word, for achieving the optimal mitigation effect, width-depth ratios greater than 5.3 and 4.3 should be applied to the spherical and Gaussian repaired contours, respectively. Particularly, when the width-depth ratios are greater than 5.3, the spherical repaired contour is preferred.

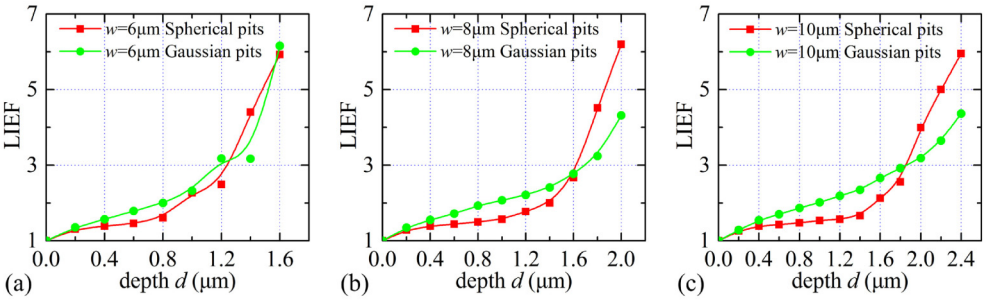

Fig. 12. Comparison of the LIEFs caused by spherical and Gaussian mitigation pits with various structural parameters. (a) w = 6μm. (b) w = 8μm. (c) w = 10μm.

4.4 Laser damage test

Figure 13 shows the comparison of measured LIDTs for KDP crystal with ideal surface and repaired surface with spherical and Gaussian mitigation pits in different sizes. Overall, the LIDTs of the four kinds of mitigation pits are close to that of the perfect surface, indicating that these mitigation pits can be applied in the actual engineering field for achieving the purpose of defect repairing. As for the difference between spherical and Gaussian contours, the LIDTs of spherical mitigation pits with the width-depth ratio of 20 and 10 are 37.69 and 35.80, respectively, which are both higher than those of Gaussian mitigation pits (36.56 and 34.41, respectively). The simulation results and analysis in Section 4.3 present that, when the width-depth ratios are larger than 5, the LIEFs of spherical mitigation pits are smaller, which means that they deserve better laser damage resistance. When it comes to quantitative analysis, the difference of LIDTs between spherical and Gaussian mitigation pits with the width-depth ratio of 20 and 10 are almost equal. In other words, these four kinds of mitigation pits get the LIDTs with slight variation. However, the gaps in the locations of width-depth ratios of 20 between the red and blue curves in Fig. 12 are larger than that of 10, which means that the Gaussian mitigation pits with width-depth ratio of 10 do not deserve such high LIDT. It is deduced that the hot spots of light intensity induced by the raster scan laser are located on the subsurface, which produce the effect similar to “laser conditioning”, especially when the light intensity is within a certain range. Thus, the mean LIDT of Gaussian mitigation pits with the width-depth ratio of 10 could be improved. By analyzing the same repairing morphology, it can be found that the LIDTs of mitigation pits with the width-depth ratio of 20 are higher than those of 10 for both the spherical and Gaussian mitigation pits. These results also agree well with the simulation results above that the LIEFs decrease with the increase of the width-depth ratio. Besides, the variation of the LIDTs between the spherical mitigation pits with the width-depth ratio of 20 and 10 presents the similar gradient to that of the LIEFs analyzed above.

Optics EXPRESS

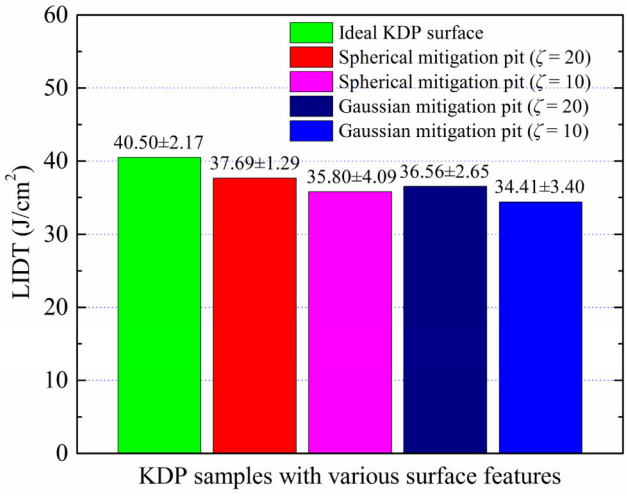

Fig. 13. Comparison of the measured LIDTs for KDP crystal with ideal surface and repaired surface with spherical and Gaussian mitigation pits in different sizes.

SEM images of damage sites around the mitigation pits on rear KDP surface initiated with 532nm light are exhibited in Fig. 14 with the insets showing the enhanced microscope images of a small region of damage. The images indicate two distinct types of damage sites. One type of damage sites, referred as "mussel" [26], is observed in large groups and generally believed to be associated with the unbearable stress induced by optical breakdown on surfaces [25]. The other type of damage sites consists of a complex core enclosed in a shell and only occupies a few points, as shown in Fig. 14(d), which is more similar to the morphology of laser-induced bulk damage (see Ref [27].). It is inferred that the precursors inside the KDP irradiated by high fluence laser with light intensification would melt or vapor first and probably be ejected from the surface of crystal to air, which finally results in formation of a "crater" site. Though different damage morphologies are related to different damage mechanisms, the light intensification inside the crystal induced by various profiles of structures would cause the local laser energy concentration, which plays an important role in driving both of these damage mechanisms. Besides, one can see that the damage area of mitigation pits with larger width-depth ratio [Figs. 14(a) and 14(c)] is smaller. The area of each damage site 10 ~30μm, and the number of damage points is less as well. As for the mitigation pits with smaller width-depth ratio [Figs. 14(b) and 14(d)], the damage area is larger with each site of 30 ~100um, and the number of damage points is larger as well. By comparing the laser damage morphologies inside the spherical and Gaussian mitigation pits, we can see that the effect of spherical mitigation pits is more obvious, especially when the width-depth ratio is relatively large. For example, even though the spherical and Gaussian mitigation pit in Figs. 14(a) and 14(c) share the same width-depth ratio, the spherical mitigation pit presents slighter laser damage. Furthermore, the laser damage on the repaired surface with Gaussian mitigation pits mainly occurs at the waist of the Gaussian curve, which also verifies the simulation results as shown in Fig. 10(b).

Optics EXPRESS

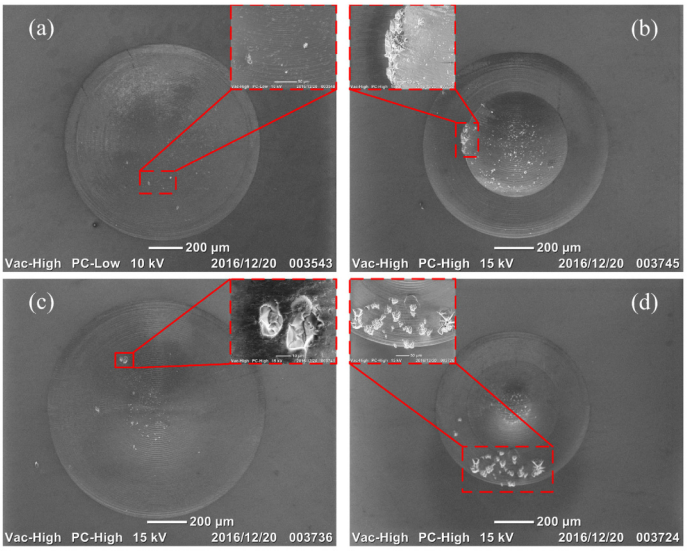

Fig. 14. SEM images of the damage sites around the mitigation pits on rear KDP surface initiated by 532nm-wavelength light. The images show the whole area of the mitigation pits with laser damage. The insets are the enhanced microscope images showing a small region of damage. (a) The spherical mitigation pit with 1000μm width and 50μm depth. (b) The spherical mitigation pit with 500μm width and 50μm depth. (c) The Gaussian mitigation pit with 1000μm width and 50μm depth. (d) The Gaussian mitigation pit with 500μm width and 50μm depth.

5. Conclusion

In this work, the effectiveness of repaired spherical and Gaussian mitigation pits on the rear surface in improving the laser damage resistance of initial damaged KDP crystal was investigated with the finite element method. By numerically simulating the distribution of electric field intensity near the repaired mitigation pit, it is found that the light intensity modulation is mainly caused by the mutual interference between the reflected and incident lights on the rear surface. The LIEFs inside the crystal depend on the structure parameters of the mitigation pits, such as width, depth and shape of the repaired contour. Due to the occurrence of total reflections at rear surface, when the width-depth ratios are close to 5.28 and 3.88 for spherical and Gaussian pits, violent light intensity modulation would appear inside the crystal. By comparing the LIEFs caused by spherical and Gaussian mitigation pits, it is recommended that the width-depth ratio greater than 5.3 and 4.3 should be applied to the spherical and Gaussian repaired contours, respectively. When the width-depth ratios are greater than 5.3, the spherical repaired contour is preferred. Besides, four series of mitigation pits were fabricated by micro-machining method and the laser damage test was implemented. The experimental results are well consistent with the simulation results by the combined consideration of the LIDTs, LIEFs and locations of laser damage and maximum hot spots. It is also proved that these mitigation pits with spherical and Gaussian contours (width-depth ratio of 20 and 10) possess high laser damage resistance. Moreover, when the width-depth ratio is larger than 5.3, the repairing effectiveness of spherical contour is better than that of Gaussian contour. These results could provide criterion for comprehensive evaluation of the repaired optical surfaces, which are beneficial to the volume fabrication and recycling of large-aperture optical components used in high power laser systems.

Funding

Science Challenge Project (JCKY2016212A506-0503); Self-Planned Task of State Key Laboratory of Robotics and System in Harbin Institute of Technology (SKLRS201718A).